SCIENTIFIC REPORTS

OPEN

SUBJECT AREAS:
MECHANICAL AND STRUCTURAL PROPERTIES AND DEVICES
ION TRANSPORT
DIAGNOSTIC MARKERS
NANOWIRES

Received
9 May 2013

Accepted
22 July 2013

Published
21 August 2013

Correspondence and requests for materials should be addressed to A.A. (abbas.amini@deakin.edu.au) or C.C. (cheng.c@sustc.edu.cn)

Nature of hardness evolution in nanocrystalline NiTi shape memory alloys during solid-state phase transition

Abbas Amini[1] & Chun Cheng[2]

[1]Institute for Frontier Materials, Deakin University, Waurn Ponds, VIC 3217, Australia, [2]Department of Materials Science and Engineering, South University of Science and Technology of China, Shenzhen, Guangdong 518055, China.

Due to a distinct nature of thermomechanical smart materials' reaction to applied loads, a revolutionary approach is needed to measure the hardness and to understand its size effect for pseudoelastic NiTi shape memory alloys (SMAs) during the solid-state phase transition. Spherical hardness is increased with depths during the phase transition in NiTi SMAs. This behaviour is contrary to the decrease in the hardness of NiTi SMAs with depths using sharp tips and the depth-insensitive hardness of traditional metallic alloys using spherical tips. In contrast with the common dislocation theory for the hardness measurement, the nature of NiTi SMAs' hardness is explained by the balance between the interface and the bulk energy of phase transformed SMAs. Contrary to the energy balance in the indentation zone using sharp tips, the interface energy was numerically shown to be less dominant than the bulk energy of the phase transition zone using spherical tips.

NiTi shape memory alloys with excellent self-control capabilities have been used in meso- and macro-scales in high tech sectors such as MEMS, lab-on-the-chips, dampers, and artificial tissues, etc[1]. Most research on these advanced alloys has focused on large scale tensile conditions[2,3]. Fundamental studies on these smart alloys under nano-scale compression loadings started recently in the wake of new technologies, i.e., nanoindentation[1]. By using this technology, the solid-state phase transition in an extremely small scale, which is the basis of the macro-scale mechanical properties, can be thoroughly investigated.

A large superelastic deformation and recovery in NiTi SMAs are originated from atomic lattice rearrangements called a discrete phase transformation[4]. In this transition, the parent austenite phase and the martensite phase revert to each other with the release or absorption of latent heat[5]. A large degree of recovery is achieved after the removal of load (pseudoelasticity) or upon the application of heat (shape memory effect)[6]. Due to the nucleation and propagation of phase transition volume during the loading and unloading stages, measuring the mechanical properties of a thermomechanical SMA, i.e., hardenss, shows a fundamental departure from the traditional approach[7,8]. This is due to the contributions of interface energy and bulk phase transition energy with the intrinsic properties which have yet to be systematically studied. In this paper, we study the trend of hardness variations in both traditional and shape memory alloys measured using spherical and sharp tips with a specific attention to the phase transition role as the main phenomenon in NiTi SMAs.

The hardness has been related to the yield stress of elastic-plastic materials by a simple three-fold relationship[9,10]. Using a sharp Berkovich or Vickers indenter, the measured hardness of ordinary materials with no phase transition decreased with the increase in the indentation depth when the depth was in a sub-micrometer regime[11,12]. This depth dependent hardness was explained by the concept of geometrically necessary dislocations and the strain gradient plasticity theory having an inverse square-root power law[13]:

$$\frac{H}{H_0} = \sqrt{1 + \frac{h^*}{h}} \tag{1}$$

where H is the hardness for a given indentation depth, h, H_0 is the hardness in the limit of infinite depth and h^* is a characteristic length that depends on the shape of the indenter, the shear modulus and H_0. For elastic-plastic materials, the measured hardness using a spherical indentation tip, here named the spherical hardness, is not sensitive to the indentation depth[14,15].

Unlike ordinary elastic-plastic materials, shape memory alloys, i.e., NiTi SMAs, react to the mechanical indentation load through a solid-state phase transition phenomenon[16–20]. An experimental and analytical study on the hardness of NiTi SMAs with a sharp Berkovich indenter was reported recently[21]. By using a total Gibbs free energy analysis of the system under a given force, the hardness decreased by increasing the depth and followed an inverse depth-dependent law:

$$\frac{H}{H_0} = 1 + \alpha\left(\frac{l}{h}\right) \qquad (2)$$

α is the lump coefficient, obtained by a curve-fitting, depending on the tip geometry and bulk properties of the NiTi SMA and l is the characteristic thickness of the interface. From Eq. (2), the depth dependence of the hardness is dictated by the ratio $\frac{l}{h}$, i.e., the smaller the depth, the higher the hardness of the material. When the depth is large enough, i.e., $\frac{l}{h} \to 0$, the measured hardness degenerates into a constant H_0 which is determined by the characteristic bulk properties and the change in the chemical free energy density. In short, the depth-dependence of the hardness for NiTi SMAs in a sharp indentation was determined by the bulk energy of the phase transformed zone in high depths and the interface energy in low depths.

The trend of the spherical hardness in superelastic NiTi SMAs shows a completely opposite trend compared to the hardness from sharp tips. In this paper, a new experimental and numerical study is conducted on the depth dependence of the spherical hardness of NiTi SMAs to explore the anomalous behaviour of the hardness increase by depth.

Results

Fig. 1 shows indentation curves for NiTi SMA from the spherical indenter with a 5 μm radius tip at room temperature. The standard tensile test (inset Fig. 1) confirms the superelasticity of the material at this temperature with the forward phase transition initiation at ~ 2.2% strain. The indentation loop curves indicate that the phase transition occurs under all specified indentation loads. When the indentation load is less than 25 mN, all the indentation depths can be significantly recovered due to the reverse phase transition during the unloading stage (see inset Fig. 1 for low indentation loads). There is only a small percentage of the residual indentation depth at larger indentation loads. No– or small residual indentation depth and a similar loading slope demonstrate that the plastic deformation and the dislocation evolution have either no– or insignificant role in this material for the selected loading range.

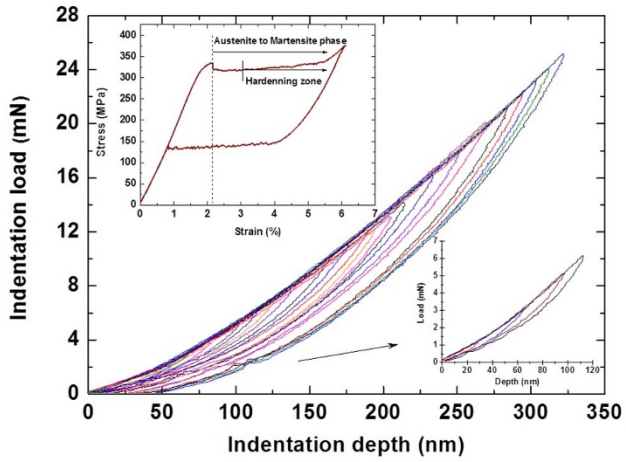

Figure 1 | Indentation curves for a NiTi shape memory alloy from spherical indentations using a 5 μm radius tip and the tensile curve (inset) at room temperature.

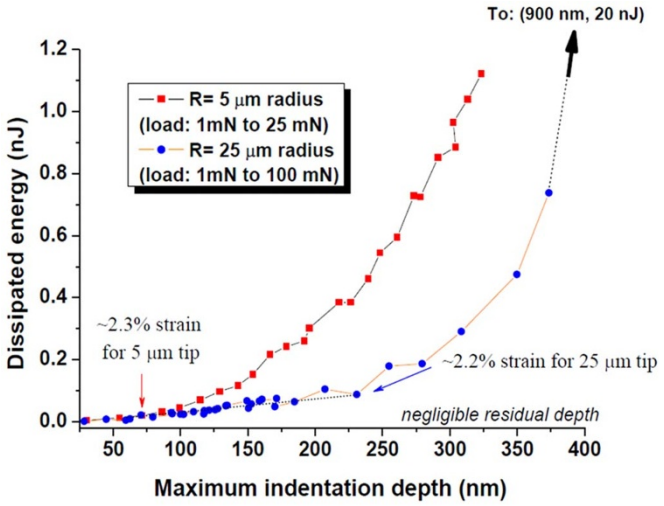

Figure 2 | Dissipated energy versus the maximum indentation force for spherical tips with radii 5 μm (loads from 1 mN to 25 mN, red squares) and 25 μm (loads from 1 mN to 100 mN, blue circles). The phase transition in the bulk starts at ~ 2.2% compressive strain (the equivalent strain) which is a similar strain to that of the tensile test for the initiation state of the phase transition.

Fig. 2 shows that the hysteresis area (dissipated energy) has a mild linear increase (to < 0.1 nanoJoules (nJ)) for shallow depths to a maximum equivalent strain of less than ~ 2.2% for 25 μm radius tip and ~ 2.3% for 5 μm radius tip. The equivalent strain in an indentation with a spherical tip is calculated by 0.2a/R. The parameter a is the contact radius calculated from $(2Rh_c - h_c^2)^{0.5}$ where R and h_c are the tip radius and the contact depth[22]. The latter is calculated by analyzing the load-displacement curve through h_{max}-0.75F_{max}/S where h_{max}, F_{max} and S are the maximum indentation depth, maximum indentation load and the slope of the tangentional line to the initial 10% portion of the unloading curve[23]. These strains are comparable with the tensile strain shown in the inset Fig. 1 (~2.2%), in which the material has undergone the linear austenite deformation before entering the phase transition zone. When the indentation depth increases, the hysteresis area shows a sharp and nonlinear increase by a sudden phase transition propagation in the bulk after ~ 2.2% strain.

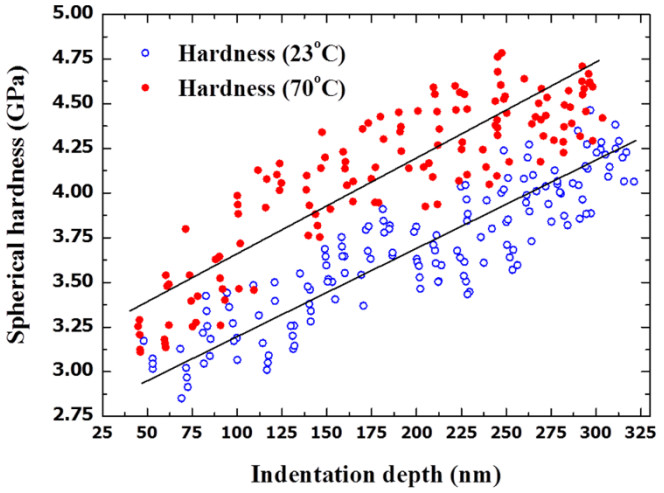

Figure 3 | The depth dependent behaviour of spherical hardness of a NiTi shape memory alloy at 23°C and 70°C in indentation tests using a 5 μm radius tip.

In Fig. 3, the spherical hardness was calculated from the measured indentation depth-load curve using the Oliver-Pharr method[23]. Although the higher phase transition stress of higher temperature results in higher spherical hardness values, however, the results show a similar trend at two temperatures, 23°C and 70°C. The spherical hardness significantly depends on the indentation depth and the average hardness value increases with the indentation depth. For instance, the average spherical hardness at room temperature, calculated from the curves in Fig. 1, increases from ~ 3 GPa at the depth of ~ 50 nm to ~ 4.5 GPa at the depth of ~ 300 nm. This depth dependent behaviour of the hardness of NiTi SMAs from a spherical indenter is opposite to that of a sharp indenter, where the hardness decreases with an increase in the indentation depth. In the following, an explanation is provided for this depth-dependent behaviour of the spherical indentation hardness.

Discussion

For a sharp indentation, the energy analysis shows that the energy of the interface between transformed martensite and original austenite phase overcomes that of the transformed bulk energy for shallow depths. This fact leads to a decrease in the hardness when the indentation depth increases due to the change of the energy balance along with the dislocation evolution underneath the tip.

To understand the opposite depth dependency of the spherical hardness, a finite element method is applied to simulate the spherical indentation tests on the NiTi SMA by using a two-step shaped stress-strain relationship. A modest plastic yield stress of 1000 MPa for the martensite phase, and an elastic moduli 20 GPa for the austenite phase and 10 GPa for the martensite phase were applied in computer simulations based on the experimental test (referring to the inset Fig. 1). The modulus of NiTi shape memory alloy strongly depends on the elastic moduli of the austenite and martensite phases, the transformation hardening coefficient, the maximum transformation strain and the forward transformation stress. Any change in these parameters would influence the magnitude of the Young's modulus of the alloy. We have used a modest amount of the elastic moduli according to these data for the present NiTi SMA. Among the various low to high magnitude of elastic moduli, a modest amount allows us to predict the behaviours of both pseudoelastic and shape memory effect alloys.

The numerical results confirmed the insignificant residual depth observed in Fig. 1 by showing that the plastic zone is no more than 5% of the phase transition zone for indentation depths less than ~ 350 nm. The low amount of plasticity is mainly due to the phase transformation volume that dominates the stressed zone underneath the spherical tip. Additionally, the contribution of the interface energy to the hardness in a spherical indentation can be evaluated numerically by the ratio of the interface volume to the phase transition volume normalized by similar data from a sharp indentation. In this way, the relative contribution of the interface energy to a spherical hardness, with respect to that in a sharp indentation, is evaluated by volume ratios. The vertical axis in Fig. 4 represents the following equality (3):

$$Relative\ V\ ratio = \left(\frac{V_{interface}}{V_{phase\ transformed\ bulk}}\right)_{\substack{spherical\\ indentation}} \Big/ \left(\frac{V_{interface}}{V_{phase\ transformed\ bulk}}\right)_{\substack{sharp\\ indentation}} \quad (3)$$

where V is the volume. In the early stage of a sharp indentation, the phase transition is mostly dominated by the interface. This fact results in a high value of the second V-ratio for a sharp indentation in the above equality. In addition, the overall relative V ratio (the left part of the above equality) starts from ~ 0.24 (Fig. 4) which implies a low amount of V-ratio for the spherical indentation. Therefore, the lower amount of the interface volume for a spherical tip in comparison with the one from a sharp tip is concluded in the early stage of the loading. For simplicity the above equality (3) is degenerated into the following equality (4):

$$Relative\ V\ ratio = \left(\frac{V_{spherical\ indentation}}{V_{sharp\ indentation}}\right)_{interface} \times \left(\frac{V_{sharp\ indentation}}{V_{spherical\ indentation}}\right)_{phase\ transformed\ bulk} \quad (4)$$

On increasing the indentation depths both bulk volumes of the phase transformation during the sharp indentation and during the spherical indentation (Fig. 2) increase when the martensite phase propagates. In higher loads, the total interface role decreases in a sharp indentation but it does not change significantly in a spherical indentation due to the energy balance. One parameter ($V_{phase\ transformed\ bulk}$ for the spherical indentation) decreases the total relative V ratio, but on the other hand, two variations in the sharp indentation (the proportinonal decrease of $V_{interface}$ and the increase of $V_{phase\ transformed\ bulk}$) result in an increase of 40% in the total relative V ratio in Fig. 4. In fact, the main controlling parameters in higher depths are phase transformed bulk volumes and the ratio of the interface volumes remains fairly unchanged. In other words, due to the higher stress concentration underneath the sharp tip than the one in a spherical indentation, more significant increase of the phase transformed volume in a sharp indentation results in the overall increase of the relative V ratio from ~ 0.24 to ~ 0.41. In short, the influence of the interface energy on the spherical indentation hardness is not significant as the one reported for the sharp indentation hardness of NiTi SMAs.

This rationale is experimentally obtained from Fig. 2 that shows the intrinsic phase transition in the bulk starts from early indentation depths. In this figure, the hysteresis area has a mild linear increase for $h < 230$ nm using 25 μm-radius tip and for $h < 50$–75 nm using 5 μm-radius tip. With the initiating phase transformation strain of ~ 2.2% (Fig. 1), the linear increase of the dissipated energy ends at ~ 2.3% strain for 5 μm-radius tip and finishes at ~ 2.2% strain for 25 μm-radius tip. In these regions, with an ignorable plasticity (work-hardening), the mild increase in the hardness originates from the elastic deformation of the original austenite phase and a small amount of the interface energy beneath the tip. It is not a coincidental that a tip with a larger radius needs more indentation depths to reach the stress required for the phase transition initiation in the bulk. In fact, the stress underneath the larger radius tip is lower in comparison with the one for similar depth using a smaller radius tip,

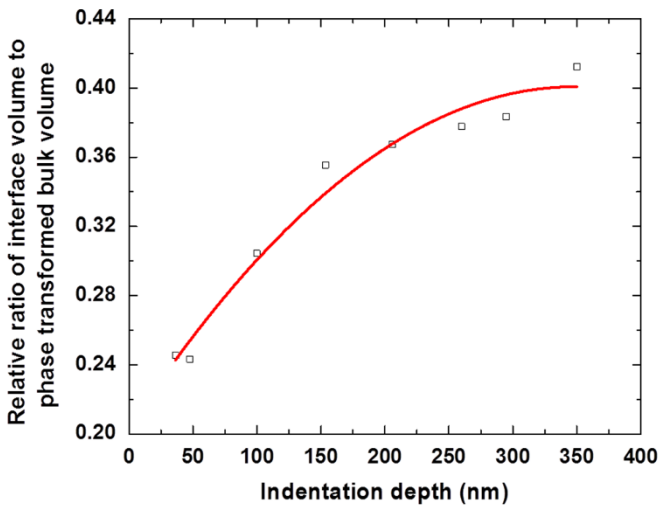

Figure 4 | Numerical results for the ratio of the interface volume to the phase transition volume from a spherical indentation, which are normalized by similar sharp indentation data at different depths.

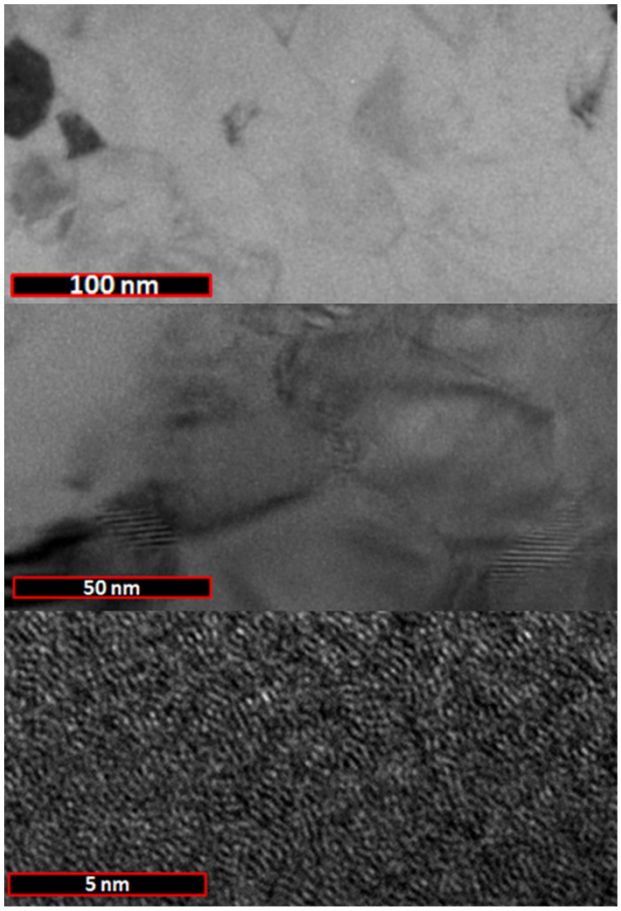

Figure 5 | **TEM images from different locations and scales of NiTi shape memory alloy's nanostructure.**

therefore, the phase transition initiation and propagation into the bulk are postponed (Fig. 2). The phase propagation occurs at the end of a low loading range ($<$ 2–3 mN). This fact confirms the significant role of the bulk transformation energy for the majority of the loading range ($>$ 3 mN). In brief, the substantial increase of the hysteresis area occurs when the applied stress overcomes the energy barrier of the interface and accumulated elastic energy of the austenite and, subsequently, the martensite phase propagates in a bulk scale.

The experimental finding of the spherical hardness behaviour (i.e., spherical hardness increase with the indentation depth) can be explained by the elastic hardness with a contribution from the phase transition. According to Hertz's theory for a purely elastic contact of a material with no phase transition, the spherical hardness H is expressed as[22]:

$$H = \frac{4}{3\pi}\frac{E}{1-\nu^2}\sqrt{\frac{h}{R}} \tag{5}$$

where E is the elastic modulus, ν is the Poisson's ratio and R is the spherical tip radius. Eq. (5) clearly indicates that the spherical hardness increases with the square root of the indentation depth for a purely linear elastic material. For NiTi SMAs, due to the elastic deformation of the austenite and martensite phases plus the large superelastic deformation during the phase transition (pseudoelasticity, Fig. 1), the above square-root law does not completely apply. However, as an elastic deformation, the elastic energy plays a dominant role and the increase in the spherical hardness with the indentation depth can still be obtained. Furthermore, compared to Eq. 5, where the hardness-depth relationship for elastic metals is proportional to $h^{0.5}$, Fig. 3 illustrates that the hardness-depth for NiTi SMAs increases linearly (proportional to h). A similar inverse transformation law can be seen between Eqs. 1 and 2, where the hardness-depth relationships for materials with no phase transformation and NiTi SMAs are proportional to $h^{-0.5}$and h^{-1}respectively.

The dislocation effect on the performance of superelastic shape memory alloys is not significant as that of other ordinary elastic-plastic materials. This originates from the stress relaxation which occurs at the front ends of the existing or created dislocations that

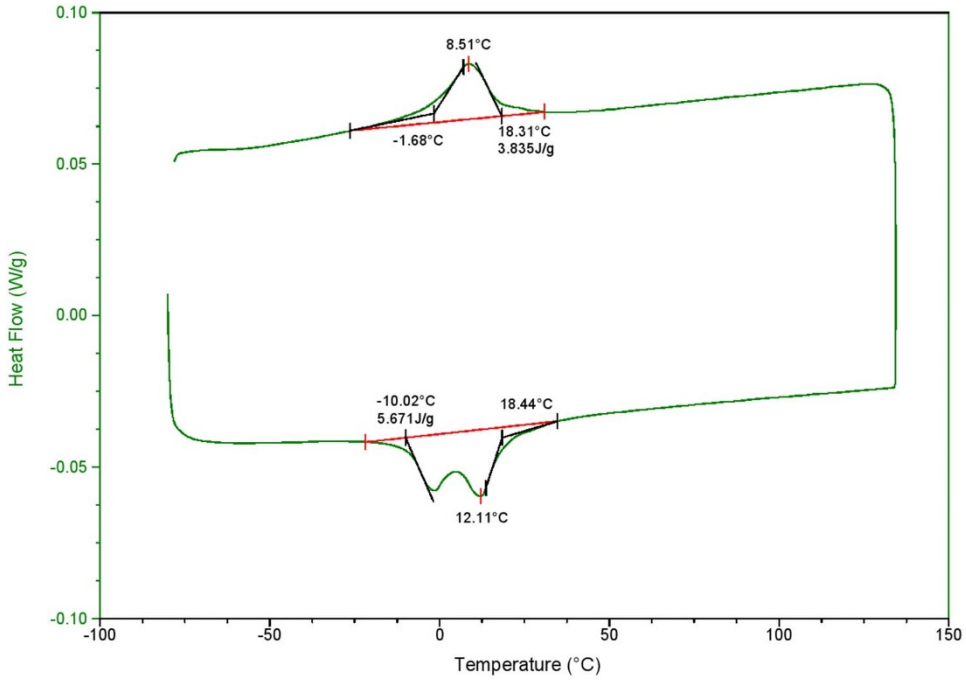

Figure 6 | **DSC curve of the NiTi shape memory alloy; the martensite finish (M_f) and start temperature (M_s), the austenite start (A_s) and finish temperature (A_f), were characterised as $M_f = -2^{\circ}C$, $M_s = 18^{\circ}C$, $A_s = -10^{\circ}C$ and $A_f = 19^{\circ}C$.**

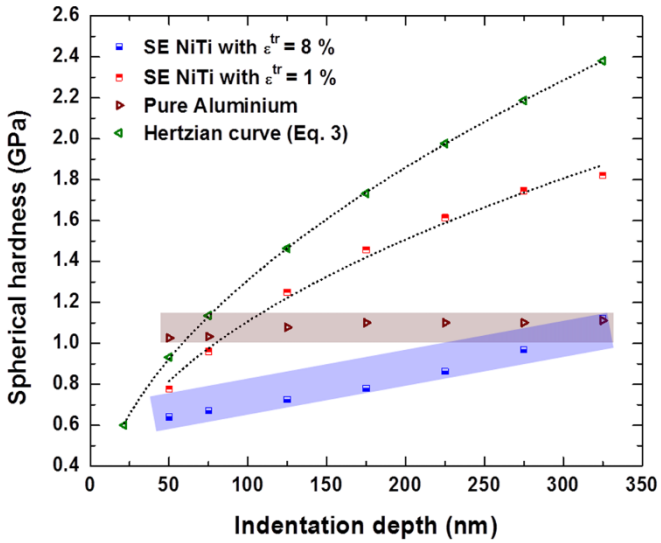

Figure 7 | Numerical results of the spherical indentation hardness to illustrate the role of the phase transition compared with the hardness of a purely elastic material and Aluminium.

results in a low effect of dislocations on the total energy of nano-scale loadings. This phenomenon can be evidenced from Fig. 1 with a low amount of residual strain. Apparently, TEM images in Fig. 5 from different locations of the alloy depict that there are no high volume of dislocations within the grains. No initial hardening during the initial 2–3% strain confirms this hypothesis (inset Fig. 1). When the load is applied at room temperature, the parent austenite phase, which mostly dominates the alloy (Fig. 6), transforms to the martensite phase rather than elevating a significant amount of dislocation volume. Inset Fig. 1 shows that during the martensite phase propagation, an insignificant hardening is observed even after 3% strain. This concludes in low volume of dislocation propagation.

The role of the deformation due to the phase transition in the depth dependent spherical hardness is illustrated in Fig. 7. Both purely elastic material and a NiTi SMA show a similar trend in hardness-depth behaviour. As discussed, the negligible interfacial energy was not included in the numerical simulations for the NiTi SMA. Under the same force, the phase transition phenomenon makes the material soft and increases the depth by a stress relaxation underneath the tip. The resultant contact area becomes larger, and therefore, the depth dependence of the hardness becomes less significant as compared to the purely elastic case. This fact is confirmed by larger phase transition strains that lead to a lower spherical hardness under the same indentation depth (Fig. 7). It is also observed that the more the phase transition strain (pseudoelasticity) is, the more the linear trend of the hardness-depth is achieved (the proportional relationship of the hardness with h, as captured by the experiment, Fig. 3).

Owing to the higher elastic modulus and the lower plastic yield strength of ordinary elastic-plastic materials, the dominated elastic deformation in a spherical indentation is too small to be captured. In other words, the spherical indentation hardness of these materials is mainly controlled by the plastic deformation, not the elastic deformation. As a result, the depth dependency of the spherical hardness due to the elastic deformation is not observed in an elastic-plastic material, e.g., Aluminium, as shown in Fig. 7. This fact leads to the depth insensitivite spherical hardness for elastic-plastic materials.

In summary, spherical indentation tests on NiTi SMAs show a significant increase in the hardness with indentation depths. This behaviour is not only opposite to the hardness decrease-depth increase behaviour of NiTi SMAs in indentation tests with sharp tips, but also it is in contrast with the depth insensitivity of the spherical hardness of ordinary materials with no phase transition. Numerical results indicate that the influence of the interface energy for NiTi SMAs, which is dominant in a sharp indentation, is relatively weak in a spherical indentation. It is further shown that the anomalous behaviour of the spherical hardness in NiTi SMAs can be explained by the elastic contact theory incorporated with the effect of the phase transition phenomenon. In NiTi SMAs, the phase transition weakens the depth dependency of the spherical hardness. This study initiates a new approach towards the hardness measurement for materials with solid-state phase transitions under different indenters at micro- and nano- scales.

Methods

Commercial polycrystalline NiTi SMA sheets were purchased from Memory Applications Inc. (USA). The size of the grain was in the range of 50–100 nm as observed by a transmission electron microscopy (TEM, JEOL JEM-2010F), Fig. 5. With a differential scanning calorimeter (DSC 92, SETARAM, France), austenite finish temperature (A_f) was measured as 19°C (Fig. 6). The material properties at room temperature (T = 23°C) were $\nu = 0.3$, $\varepsilon^{tr} = 3.5\%$, $\sigma_f = 325\ MPa$ (inset Fig. 1). ν, ε^{tr} and σ_f represent the Poisson's ratio, the maximum transformation strain and the forward phase transition stress of the material. The sheets were cut into 5 mm × 5 mm pieces and polished by a series of silicon carbide papers and diamond papers using aluminium oxide suspensions with a minimum grain diameter of 0.05 μm until the average surface roughness was less than 6 nm checked by a 3D surface profiler (SPM NT3300, Wyko, USA). Before the experiments, the materials were heated to 100°C for one hour and then gradually cooled down to room temperature so that a 100% austenite phase was retained. Nanoindentation tests were conducted in a quasi-static mode at room temperature and 70°C by a Wrexham machine (UK). This machine had two self-feedback heating stages for both the material and the tip to conduct the tests at higher temperatures. This helped to minimize the thermal drift of the tip during the tests. The pre-installed isolation shields in the machine prevented any thermal interference with the ambient, electronics and depth sensing equipment. Before the indentation test at the aimed temperatures the machine was carefully calibrated according to the standard procedure. Using an electronic self-checking pulse, the hot stage controlled and raised the temperature slowly with a set ramp rate of 1°C/min to achieve the desired temperature, i.e., 70°C. The test was performed after thirty minutes of this raising process to make sure both tip and the mounted sample were in a thermal equilibrium state. Once these values were set, the resultant schedule was analysed as normal, i.e., high temperature data was analysed in the same way as room temperature data.

Simple loading and unloading schemes were applied with low loading and unloading rates to avoid the rate effect. The maximum indentation loads in the tests were from 1 mN to 25 mN with a constant rate of 1 mN/sec using a spherical indenter of 5 μm tip radius, and from 1 mN to 100 mN with a similar rate using a spherical indenter of 25 μm tip radius. The load magnitudes were selected to avoid or minimize the plastic deformation.

The tensile test was performed at room temperature on a dog-bone shape NiTi strip of the total length of 60 mm, 10 mm-width head and 0.5 mm thickness prepared by a wire-cutting machine. The middle portion of the strip had 30 mm length and 2.6 mm width. The wire-cut process was performed under a coolant with a low feed rate, however, before the tensile test, the edge of the sample was carefully grinded by a 1200 μm sand paper to minimize the surface roughness and possible crack zones. A low nominal strain rate of 0.5×10^{-4}/sec was selected in a constant magnitude throughout the loading and unloading stages to preserve an isothermal and rate-independent condition[21].

1. Amini, A. *et al.* Effect of graphene on thermomechanical behaviour of NiTi shape memory alloy during nano-scale phase transition. *Scripta Mater.* **68**, 420–423 (2012).
2. Caballero, V. & Varma, S. Effect of stacking fault energy and strain rate on the microstructural evolution during room temperature tensile testing in Cu and Cu-Al dilute alloys. *J. Mater. Sci.* **34**, 461–468 (1999).
3. Bruno, O. P., Leo, P. H. & Reitich, F. Free Boundary Conditions at Austenite-Martensite Interfaces. *Phys. Rev. Lett.* **74**, 746–749 (1995).
4. Frick, C. P., Lang, T. W., Spark, K. & Gall, K. Stress-induced martensitic transformations and shape memory at nanometer scales. *Acta Mater.* **54**, 2223–2234 (2006).
5. Amini, A., Cheng, C. & Asgari, A. Combinational rate effects on the performance of nano-grained pseudoelastic Nitinols. *Mater. Lett.* **105**, 98–101 (2013).
6. Igata, N., Urahashi, N., Sasaki, M. & Kogo, Y. High damping capacity due to two-step phase transformation in Ni–Ti, Ni–Ti–Cu, and Fe–Cr–Mn alloys. *J. Alloys Compd.* **355**, 85–89 (2003).
7. Amini, A., Beladi, H., Hameed, N. & Will, F. Effects of dynamic loading on nano-scale depth-recovery and damping property of single crystal CuAlNi shape memory alloy. *J. Alloys Compd.* **545**, 222–224 (2012).

8. Ma, X. G. & Komvopoulos, K. Pseudoelasticity of shape-memory titanium–nickel films subjected to dynamic nanoindentation. *Appl. Phys. Lett.* **84**, 4274–4276 (2004).
9. Archard, J. Contact and rubbing of flat surfaces. *J. Appl. Phys.* **24**, 981–988 (1953).
10. Tabor, D. *The hardness of metals.* (Clarendon Press, 1951).
11. McElhaney, K., Vlassak, J. & Nix, W. Determination of indenter tip geometry and indentation contact area for depth-sensing indentation experiments. *J. Mater. Res.* **13**, 1300–1306 (1998).
12. Ma, Q. & Clarke, D. R. Size dependent hardness of silver single crystals. *J. Mater. Res.* **10**, 853–863 (1995).
13. Nix, W. D. & Gao, H. Indentation size effects in crystalline materials: a law for strain gradient plasticity. *J. Mech. Phys. Solids* **46**, 411–425 (1998).
14. Huang, Y. *et al*. A model of size effects in nano-indentation. *J. Mech. Phys. Solids* **54**, 1668–1686 (2006).
15. Swadener, J., George, E. & Pharr, G. The correlation of the indentation size effect measured with indenters of various shapes. *J. Mech. Phys. Solids* **50**, 681–694 (2002).
16. Buschbeck, J., Kawasaki, J., Kozhanov, A., James, R. & Palmstrøm, C. Martensite transformation of epitaxial Ni–Ti films. *Appl. Phys. Lett.* **98**, 191901 (2011).
17. Ezaz, T. & Sehitoglu, H. Type II detwinning in NiTi. *Appl. Phys. Lett.* **98**, 141906 (2011).
18. Hao, S. *et al*. The ultrahigh mechanical energy-absorption capability evidenced in a high-strength NbTi/NiTi nanocomposite. *Appl. Phys. Lett.* **99**, 024102 (2011).
19. Li, Y.-H., Rao, G.-B., Rong, L.-J. & Li, Y.-Y. The influence of porosity on corrosion characteristics of porous NiTi alloy in simulated body fluid. *Mater. Lett.* **57**, 448–451 (2002).
20. Shaw, G. A., Trethewey, J. S., Johnson, A. D., Drugan, W. J. & Crone, W. C. Thermomechanical High-Density Data Storage in a Metallic Material Via the Shape-Memory Effect. *Adv. Mater.* **17**, 1123–1127 (2005).
21. Amini, A. *et al*. Temperature variations at nano-scale level in phase transformed nanocrystalline NiTi shape memory alloys adjacent to graphene layers. *Nanoscale.* **5**, 6479–6484 (2013).
22. Johnson, K. L. *Contact mechanics.* (Cambridge university press, 1987).
23. Oliver, W. C. & Pharr, G. M. Improved technique for determining hardness and elastic modulus using load and displacement sensing indentation experiments. *J. Mater. Res.* **7**, 1564–1583 (1992).

Acknowledgments

The Hong Kong Research Grants Council for partially supporting this study through a CERG grant under the RGC projects (No. 620109 and No. 619511) and South University of Science and Technology of China for providing the starting grants are greatly acknowledged. The authors also would like to thank Dr. Wenyi Yan for performing the computational simulations through the NCI National Facility in Canberra, Australia and Dr. Pavel Cizek for his valuable comments on TEM results.

Author contributions

A.A. designed the experiments, wrote the paper, performed the nanoindentation and TEM tests and analysed the results. C.C. performed the DSC and material characterisation, and incorporated on TEM interpretation and the paper revision.

Additional information

Competing financial interests: The authors declare no competing financial interests.

How to cite this article: Amini, A. & Cheng, C. Nature of hardness evolution in nanocrystalline NiTi shape memory alloys during solid-state phase transition. *Sci. Rep.* **3**, 2476; DOI:10.1038/srep02476 (2013).

SCIENTIFIC REPORTS

DOI: 10.1038/srep03316

SUBJECT AREAS:
MECHANICAL AND STRUCTURAL PROPERTIES AND DEVICES
ION TRANSPORT
DIAGNOSTIC MARKERS
NANOWIRES

SCIENTIFIC REPORTS:
3 : 2476
DOI: 10.1038/srep02476
(2013)

Published:
21 August 2013

Updated:
22 November 2013

CORRIGENDUM: Nature of hardness evolution in nanocrystalline NiTi shape memory alloys during solid-state phase transition

Abbas Amini & Chun Cheng

There is a typographical error in Figure 7 of this Article. "Hertzian curve (Eq. 3)" should read "Hertzian curve (Eq. 5)". The correct Figure 7 appears below as Figure 1.

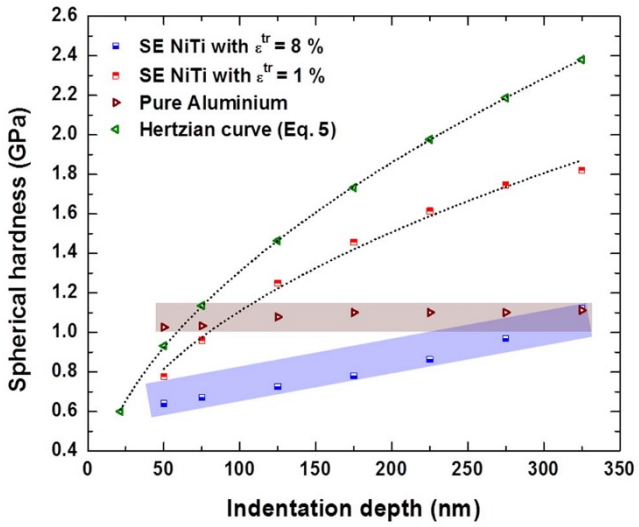

Figure 1 |